Roughening for Strengthening and Toughening in Monolayer Carbon Based Composites

Wenhui Xie and Yujie Wei*

Read Online

ACCESS | Metrics & More | Article Recommendations

ABSTRACT: Three-dimensional (3D) aggregation of graphene is dramatically weak and brittle due primarily to the prevailing interlayer van der Waals interaction. In this report, motivated by the recent success in synthesis of monolayer amorphous carbon (MAC) sheets, we demonstrate that outstanding strength and large plastic-like strain can be achieved in layered 3D MAC composites. Both surface roughening and the ultracompliant nature of MACs count for the high strength and gradual failure in 3D MAC. Such properties are not seen when intact graphene or multiple stacked MACs are used as building blocks for 3D composites. This work demonstrates a counterintuitive mechanism that surface roughening due to initial defects and low rigidity may help to realize superb mechanical properties in 3D aggregation of monolayer carbon.

KEYWORDS: *Monolayer amorphous carbon, Graphene, Roughening, Toughness, Strength*
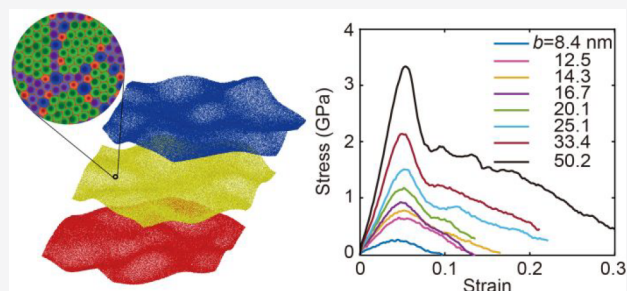
The scale-up of two-dimensional (2D) graphene sheets as building blocks for 3D materials with comparable properties to those of graphene has received enormous attention. A strong incentive comes from the ultrahigh in-plane strength of graphene[1,2] and the success of carbon-fiber and carbon-tube reinforced composite materials.[3−7] Theoretically, hybrid carbon nanofoam structures[8−10] with a mixture of sp[2] and sp[3] bonding nature may owe strength close to 2D graphene. Experimental evidence also points to the possibility of 3D carbon honeycomb.[11] The strict conditions to achieve stable 3D structures[12,13] make its scale-up a mission hard to attain.

The traditional way of making paper, for its great advantages in engineering practice, was explored. Several papers have reported the mechanical properties of graphene paper[14−22] and multilayered graphene−polymer composites.[23−25] While promising properties may be realized, they are in no way comparable to either graphene or carbon nanotubes (CNTs). The cause is again due to poor interlayer bonding. Theoretically, if graphene layers are in line with the loading direction, we would expect very appealing strength in such composites. As analyzed by Gao et al.,[26,27] tensile load on the graphene sheet may be shifted to its adjacent neighbors via interfacial shearing, a bioinspired design motif when strong blocks and compliant interfaces are assembled in an alternative manner.

Recent success in making strong steel-like, nanowood cellulose-based composites with the paper-making routine underpinned the effectiveness of the aforementioned design motif.[28] It is essential, as the authors stated, to have cellulose

fibers down to the nanoscale, where interfacial bonding between fibers is more reliable and stronger. Back to the stacked graphene, as its thickness is down to the bottom, other mechanisms ought to be engineered in order to enhance interfacial bonding. Many ways, including bringing in high cohesive bonding between graphene sheets and polyurethane segments,[6,29,30] that introduce oxygen functional groups by modifying graphene via physical or chemical treatments, known as graphene oxide (GO),[31−36] were employed to enhance interlayer contact and interactions. Those methods are very helpful in improving the deformability of graphene-based composites. Nevertheless, the strength of graphene composites[31,35,37] reported from the literature is still far less than that of graphene[1] by 2 to 3 orders of magnitude.

Surface morphologies, including thermally induced wrinkles and out-of-plane deformation by intrinsic defects, are known to play an important role in tailoring the mechanical and physical properties of graphene.[38−45] Very recently, 2D free-standing monolayer amorphous carbon (MAC) was reported[46] by laser-assisted chemical vapor deposition. MAC can be synthesized in centimeter scale, continuously and stably, with randomly distributed crystallites surrounded by five-, six-, seven-, and
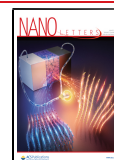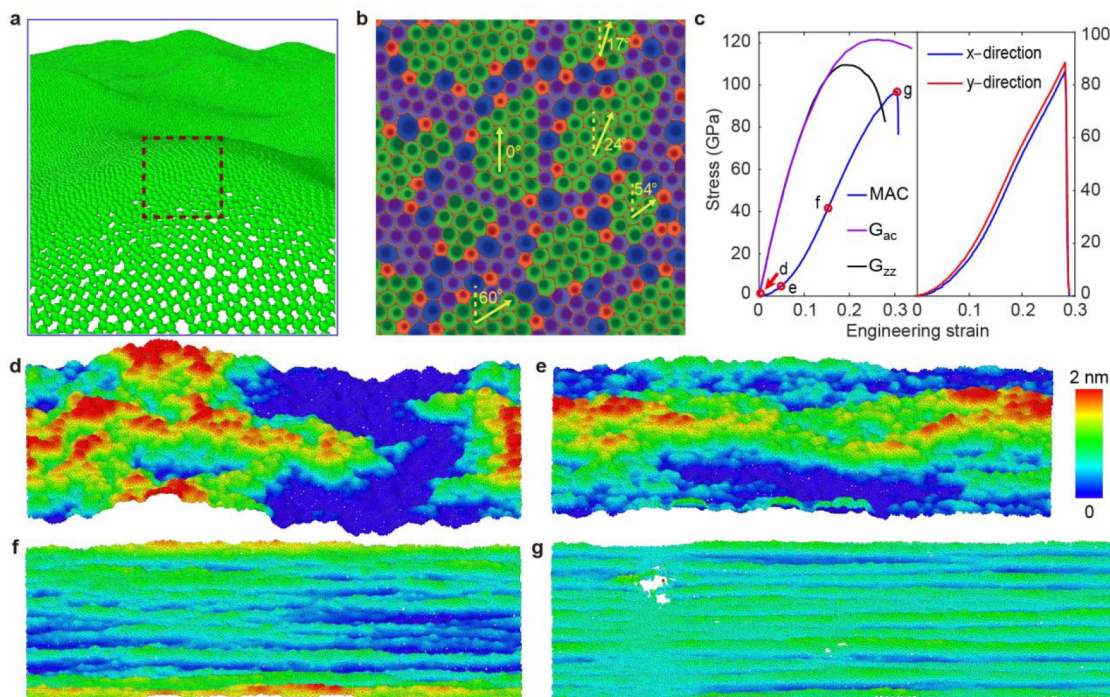
Figure 1. Atomic structure and tensile simulations of MAC. (a) Surface topography of a MAC at relaxed state. (b) Atomic network of the selected region in (a). Crystallites (in green, defined to consist of at least a hexagonal ring surrounded by six hexagonal rings) surrounding with five- (red), six- (purple), seven-, and eight-membered rings (blue). The orientations of the crystallites are random, as described by the arrows and the angle w.r.t. the vertical direction. (c) Uniaxial (left) and biaxial (right) tensile stress−strain curves of the MAC. For comparison, the responses of pristine graphene along the armchair (G_{ac}) and the zigzag (G_{zz}) direction from DFT calculations[47] are reproduced. (d−g) Sequence of snapshots at different strains keyed in (c): (d) $\varepsilon = 0$, (e) $\varepsilon = 0.05$, (f) $\varepsilon = 0.15$, and (g) $\varepsilon = 0.3$.
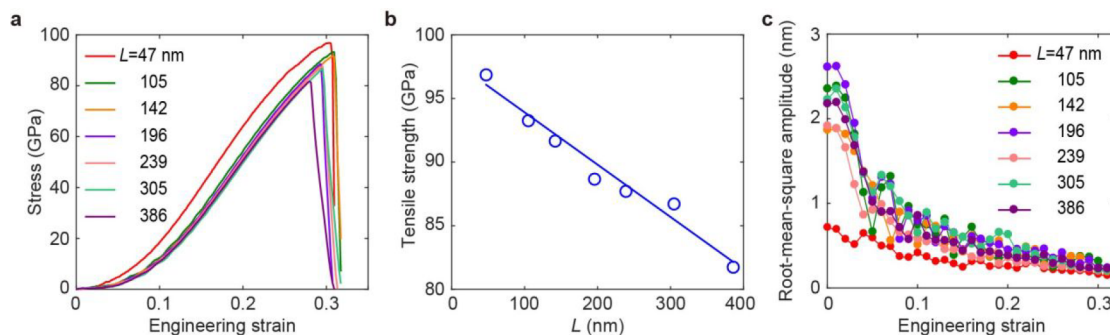

Figure 2. Size-dependent mechanical behavior of MAC sheets. (a) Stress−strain curves of samples of different length. (b) Tensile strength as a function of sample length L. (c) Root-mean-square amplitude in MAC samples as a function of strain.

eight-membered rings. Using molecular dynamics (MD) simulations (see Materials and Methods for details), we show in this report that defect-induced roughening plays a pivotal role in increasing the interaction between MAC layers. In combination with the ultracompliant nature of single-layer MAC, high strength and plastic-like deformation can be achieved in 3D MAC.

Figure 1a,b shows the typical morphology of a MAC and the close-up view of atomic network of the MAC, respectively. Due to high density of defects, its out-of-plane deformation can be on the order of nanometers. The roughening and the compliance of MAC borne from the atom-thick structure may help to realize shear shifting, a foundation for better strength and ductility in layered materials. It is worth noting that a MAC is nearly as strong as intact graphene, as demonstrated in Figure 1c. The strengths in both uniaxial tension and biaxial tension of a MAC are about 90 GPa, in

contrast to the 110 GPa strength of intact graphene. The strain-to-fracture of the MAC sample is also similar to that of graphene. The surface morphologies of the sample (47.3 nm by 26.8 nm of its initial length and width) are shown in Figure 1d−g. Those snapshots from our MD simulations correspond to strain-free, 5%, 15%, and 30% strains, in turn. The nonlinear stress−strain responses of a MAC in the low-strain regime up to 10% (Figure 1c) come from the initially rough surface, as seen in Figure 1d. With increasing tensile strain, the rough surface flattens, with a string of longitudinal wavy stripes emerging at ~15% strain (see Figure 1f). The sample can be stretched up to ~30% strain until failure (Figure 1g).

Given the highly populated "defects" in MAC and the broad interest in defect- and size-dependent mechanical property in graphene,[40,41,44,48−55] we first show in Figure 2a the stress−strain curves of MAC samples of constant width $W = 26.8$ nm and different length L. We can see that the stress−strain
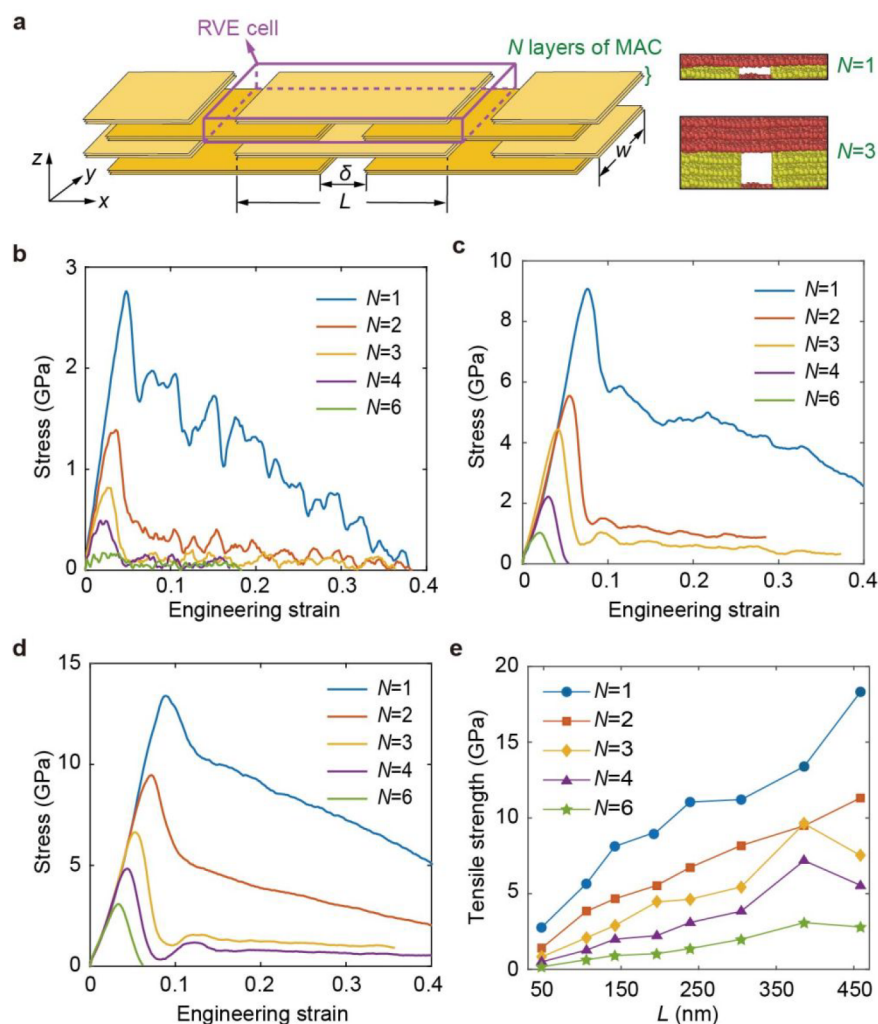
Figure 3. Mechanical behavior of the stacked MAC sheets. (a) Schematics of the architected hierarchical composites (left) and the atomic structures of building blocks with $N = 1$ and 3 (right). (b–d) Stress–strain curves of three types of samples with (b) $L = 47.3$ nm, (c) 195.8 nm, and (d) 385.9 nm. For each L, the influence of MAC layers N in building blocks is shown. (e) Strength as a function of L for different N.

responses of all samples are similar and they have a fracture strain up to 30%. In Figure 2b, we plot the tensile strength as a function of sample length L. Larger samples may have greater probability of critical defects to trigger high stress concentration, and hence growth and coalescence of small defects and eventual failure. This mechanism is akin to what we observe in ceramics, which gives rise to a linear increasing of strength as L varies from 400 to 50 nm, as we see from Figure 2b. We also track the root-mean-square (RMS) amplitude of the out-of-plane deformation in samples of different length, as shown in Figure 2c. Almost all samples have an initial out-of-plane RMS on the order of 2 nm, and RMS decreases as a resultant of flattening of samples subject to increasing tension, as illustrated in Figure 1d–g.

For a graphene sheet of thickness $t = 3.35$ Å, its uniaxial tensile strength σ_f is about 110 GPa,[47] contrary to an interfacial shear strength τ_f as low as 0.04 MPa.[56] The characteristic length l_t for efficient interfacial load transfer is estimated to be $l_t = \sigma_f t / \tau_f$[30] which is on the order of 1 mm. To the best scenario, for graphene flakes whose size is close to or greater than l_t and with effective interfacial load-shifting, we may utilize the full in-plane strength of graphene. The opposite low strength in most "graphene paper" may imply poor interlayer

bonding. Stacking with MACs, due to both surface roughness and its compliant nature, could then bring in new phenomena.

As show in Figure 3a, we designed a hierarchical composite composed of one type of uniform building blocks. In each block, it includes $2 \times N$ layers of MAC, and all MAC layers have the same length L and width $w = 26.8$ nm (in the transverse direction). The right-hand side of Figure 3a shows the side view of two types of cells, with $N = 1$ at the top and $N = 3$ for the bottom one. We intentionally leave a clearance of $\delta \sim 1.5$ nm between adjacent flakes in the horizontal direction to avoid chemical bonding between neighboring layers. The interlayer spacing is set to be 3.35 Å initially, which will then evolve due to the interplay between thermal undulation and interlayer interaction. We explore two geometrically related features during stacking: N the thickness of the building block and L its length. Interlayer interaction between MAC sheets is the same van der Waals interaction adopted for graphene layers.[56−60]

In Figure 3b–d, we show the stress–strain curves of MAC composites constructed by building blocks of $L = 47.3$ nm, 195.8 and 385.9 nm, respectively. For each type of building block, we explore the influence of layer number N on the composites. Mechanically, it reflects the flexibility of a building
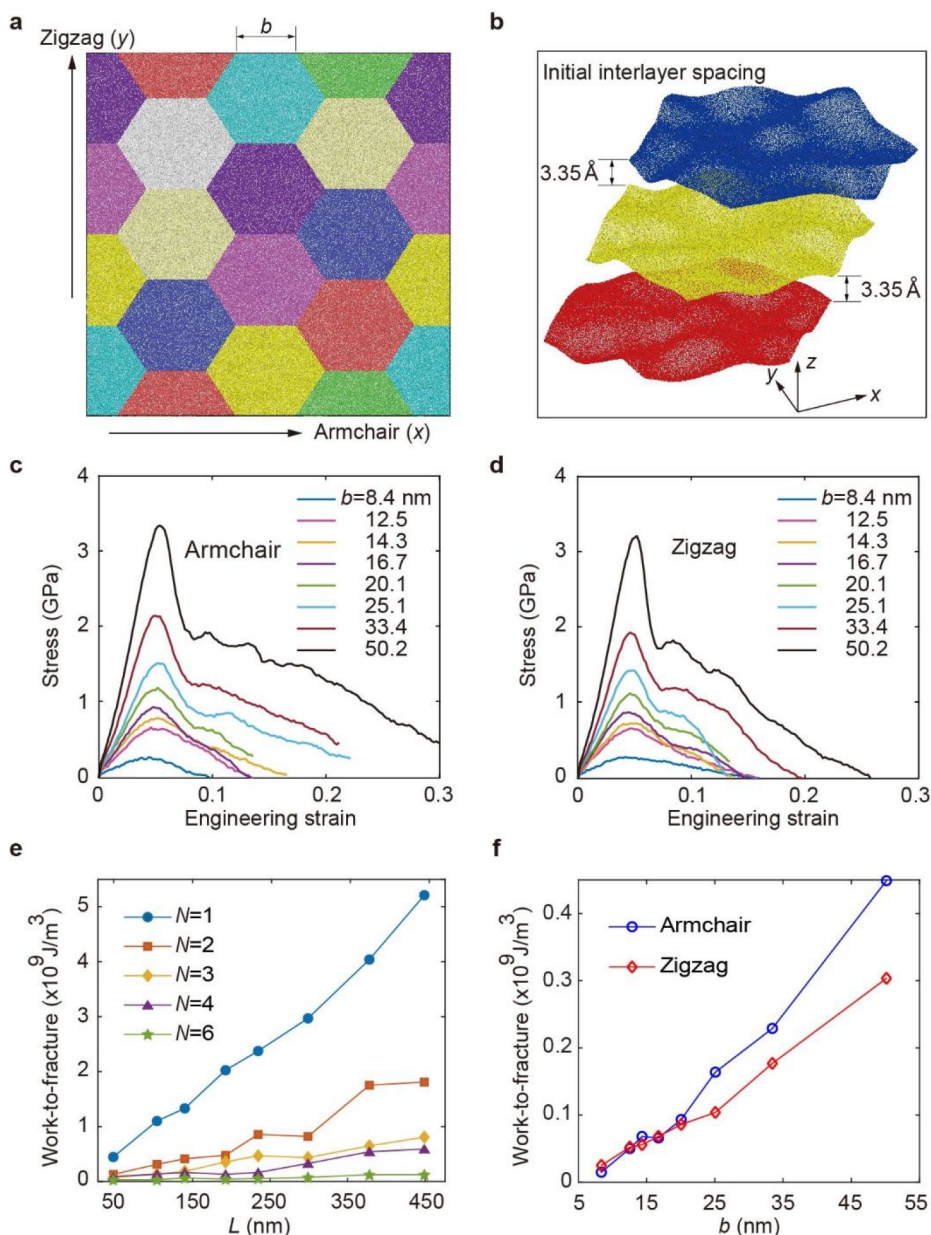
Figure 4. Mechanical behavior of the stacked hexagonal MAC sheets. (a) Top view and (b) side view of the stacked hexagonal MAC sheets structure. The hexagonal side is *b*, and the initial interlayer spacing is 3.35 Å. (c,d) Stress−strain curves along the armchair and the zigzag direction, respectively. Work-to-fracture of rectangular (e) and hexagonal (f) samples.

block. To exclude any possible size effect, all samples in our simulations contain the same amount of MAC layers so that the thickness is the same. For a sample containing 24 MAC layers, five different thicknesses are explored here. For samples of different *L*, the tensile strength of *N* = 1 is much higher than the others. Other than the expected abrupt failure after the peak stress, the stress−strain responses here, for almost all samples and in particular when *N* = 1, show that the materials exhibit plastic-like deformation. The tensile strength increases with the increasing sheet length as shown in Figure 3e, which is attributed to improved interlayer load-shift due to roughening and flexibility. These two distinct mechanisms, one arising from defects and the other due to the ultrathin layer stacking, may be intertwined, as decreasing flexibility (increasing *N*) will reduce roughening, either by defects or due to thermal undulation.

Based on the information from Figure 2b and Figure 3e, we may estimate a transitional length L_c when the strength of a MAC equals the shear stress. Considering a linear relationship between the tensile strength and the sheet length *L*, as shown in Figure 2b, we may write the failure strength σ_f as
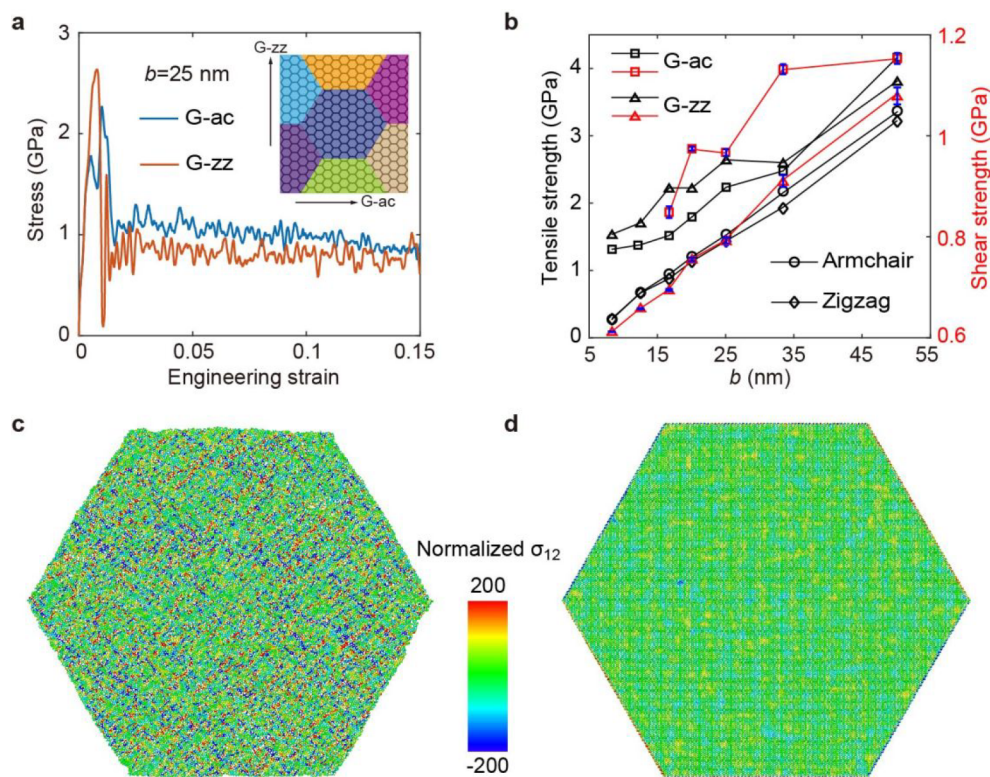
$$\sigma_f = \sigma_0 + k \cdot L \tag{1}$$

where σ_0 is the strength when extrapolating *L* to 0 in Figure 2b, and *k* is the slope of the curve. The transitional length can be estimated to be

$$\sigma_f \cdot w \cdot t = \tau_f \cdot (L_c - \delta) \cdot w \tag{2}$$

Since δ is a constant and is far less than L_c, we have

$$L_c = \sigma_0 t \big/ (\tau_f - kt) \tag{3}$$

Figure 5. Mechanical behavior of stacked MAC and stacked graphene. (a) Stress−strain curves along the armchair and the zigzag directions (b = 25 nm). (b) Tensile strength (black lines) and shear strength (red lines with error bars) as a function of sheet size. (c,d) Normalized shear stress contour in representative 3D composites subject to tension: (c) in a MAC and (d) in a graphene.

For w = 26.8 nm, $\sigma_0 \approx 98$ GPa, and $k \approx -0.04$ from Figure 2b, we have $L_c \approx 2.5$ μm. To see the strength plateau in Figure 3e, simulations with L up to several microns have to be performed.

We note that these rectangular sheets introduce a length to width aspect ratio. To ensure the robustness of this observation shown in Figure 3, we further use hexagonal MAC sheets, as shown in Figure 4a. We set an initial interlayer spacing of 3.35 Å (see Figure 4b) and follow the ACBACB⋯ stacking for MAC sheets along the z-axis, similar to the atomic-scale ACB⋯ layers in graphite.[61]

Figure 4c,d shows the stress−strain responses of the stacked structures in the armchair and the zigzag direction, respectively. The mechanical behaviors in both directions are similar, and the tensile strength in the armchair direction is slightly higher than that in the zigzag direction, like the mechanical responses of pristine graphene (Figure 1c, left). Both the strength and the fracture strain increase with sheet size b. Similar to the rectangular stacking structure, the transitional size b_c for hexagonal MAC layers may be estimated as

$$\sigma_f \cdot \bar{w} \cdot t = \tau_f \cdot \left(\frac{3\sqrt{3}}{2} \right) b_c^2 \tag{4}$$

Here, $\bar{w}$ is the equivalent width of the hexagonal sheets and is about $1.5b$. Therefore, the critical size for the hexagonal sheet is $b_c = 1.2$ μm. The work-to-fracture of the two stacking strategies increases with greater sheet size, as shown in Figure 4e for L and Figure 4f for b. Moreover, it is clearly shown in the rectangular building blocks that excellent fracture resistance can be obtained when $N = 1$ (see Figure 4e).

For comparison, stacked structures with hexagonal pristine graphene sheets (to replace those MAC sheets in Figure 4) are

investigated. Their mechanical behaviors are presented in Figure 5. Here, we set the armchair direction at the atomic scale in a graphene sheet coincide with the armchair direction of the sheets (see the inset in Figure 5a).

The stress exhibits an abrupt drop after a linear elastic region up to ∼1% strain, followed by slip−stick deformation. We show in Figure 5b the strength of these two stacked structures in the armchair and the zigzag direction. Black lines are for tensile strength, while red lines with error bars represent shear strength. Both types of stacked structures shown in Figures 4 and 5 fail by interfacial sliding. However, MAC has a much rougher surface than that of graphene. The highly populated defects lead to large out-of-plane deformation and widely distributed nanoscale wrinkles in MAC layers. Upon straining, those wrinkles bring in heterogeneous yet small-scale interfacial slips, consequentially heterogeneous distribution of shear stress (see Figure 5c). By contrast, shear stress is nearly uniform (Figure 5d) in the 3D composite by stacking hexagonal graphene sheets. It then leads to abrupt drop in stress and also localized deformation, in contrast to small-scale plastic deformation accommodated by nanoscale wrinkles. Defects in MAC and its 3D composites are thermally stable at room temperature, which may suggest excellent fatigue performance, as seen in its graphene counterpart.[62]

In summary, starting from the key issues of scale-up, we explore the influence of roughness and flexibility of atomic-layer carbon on the mechanical properties of their stacked 3D composites. Counterintuitively, defect-rich monolayer amorphous carbon sheets, when stacking up layer by layer, can reach extremely high strength on the order of several gigapascals. Opposite to most other stacked hierarchical structures exhibiting abrupt or progressive failure, MAC layered materials

show plastic-like deformation after the peak stress, which leads to high work-to-fracture. Such mechanical behavior is also sensitive to the thickness of building blocks so that the thinner blocks give rise to higher strength and more gradual failure. It is clear that both surface roughening and out-of-plane flexibility of MAC are the key factors contributing to the high strength and gradual failure in 3D MAC. The conclusions seem to be general for other types of atomic-scale films, and our results present a new strategy in enhancing toughness in van der Waals heterostructures to effectively avoid catastrophic failure.

■ MATERIALS AND METHODS

The MD package LAMMPS[63] is adopted for our calculations. All monolayer MD simulations are performed using the NPT ensemble for structure relaxation and NVT ensemble for stretching, and the system is maintained at 300 K. The periodic boundary condition is applied along the horizontal and vertical directions, and no constraint is applied to the thickness direction for the simulation box. For all simulations, the Adaptive Intermolecular Reactive Empirical Bond Order (AIREBO) Potential[64] for Carbon and a constant time step of 1 fs are used. All samples are strained at a constant strain rate of 10^9 S^{-1}.

■ AUTHOR INFORMATION

Corresponding Author

Yujie Wei − *LNM, Institute of Mechanics, Chinese Academy of Sciences, Beijing 100190, People's Republic of China; School of Engineering Sciences, University of Chinese Academy of Sciences, Beijing 100049, People's Republic of China;* ⓞ orcid.org/0000-0002-3213-7891; Email: yujie_wei@lnm.imech.ac.cn

Author

Wenhui Xie − *LNM, Institute of Mechanics, Chinese Academy of Sciences, Beijing 100190, People's Republic of China; School of Engineering Sciences, University of Chinese Academy of Sciences, Beijing 100049, People's Republic of China*

Complete contact information is available at:
https://pubs.acs.org/10.1021/acs.nanolett.1c01462

Notes

The authors declare no competing financial interest.

■ ACKNOWLEDGMENTS

■ REFERENCES

(1) Lee, C.; Wei, X.; Kysar, J. W.; Hone, J. Measurement of the elastic properties and intrinsic strength of monolayer graphene. *Science* **2008**, *321*, 385−388.

(2) Cao, K.; Feng, S.; Han, Y.; Gao, L.; Hue Ly, T.; Xu, Z.; Lu, Y. Elastic straining of free-standing monolayer graphene. *Nat. Commun.* **2020**, *11*, 284.

(3) Andrews, R.; Jacques, D.; Rao, A. M.; Rantell, T.; Derbyshire, F.; Chen, Y.; Chen, J.; Haddon, R. C. Nanotube composite carbon fibers. *Appl. Phys. Lett.* **1999**, *75*, 1329−1331.

(4) Ajayan, P. M.; Schadler, L. S.; Giannaris, C.; Rubio, A. Single-walled carbon nanotube-polymer composites: strength and weakness. *Adv. Mater.* **2000**, *12*, 750−753.

(5) Coleman, J. N.; Khan, U.; Blau, W. J.; Gun'ko, Y. K. Small but strong: A review of the mechanical properties of carbon nanotube-polymer composites. *Carbon* **2006**, *44*, 1624−1652.

(6) Huang, X.; Qi, X.; Boey, F.; Zhang, H. Graphene-based composites. *Chem. Soc. Rev.* **2012**, *41*, 666.

(7) Filleter, T.; Espinosa, H. D. Multi-scale mechanical improvement produced in carbon nanotube fibers by irradiation cross-linking. *Carbon* **2013**, *56*, 1−11.

(8) Kuc, A.; Seifert, G. Hexagon-preserving carbon foams: Properties of hypothetical carbon allotropes. *Phys. Rev. B: Condens. Matter Mater. Phys.* **2006**, *74*, 214104.

(9) Zhao, Z.; Xu, B.; Wang, L.-M.; Zhou, X.-F.; He, J.; Liu, Z.; Wang, H.-T.; Tian, Y. Three dimensional carbon-nanotube polymers. *ACS Nano* **2011**, *5*, 7226−7234.

(10) Zhu, Z.; Tománek, D. Formation and stability of cellular carbon foam structures: an ab initio study. *Phys. Rev. Lett.* **2012**, *109*, 135501.

(11) Krainyukova, N. V.; Zubarev, E. N. Carbon honeycomb high capacity storage for gaseous and liquid species. *Phys. Rev. Lett.* **2016**, *116*, 055501.

(12) Pang, Z.; Gu, X.; Wei, Y.; Yang, R.; Dresselhaus, M. S. Bottom-up design of three-dimensional carbon-honeycomb with superb specific strength and high thermal conductivity. *Nano Lett.* **2017**, *17*, 179−185.

(13) Zhang, Z.; Kutana, A.; Yang, Y.; Krainyukova, N. V.; Penev, E. S.; Yakobson, B. I. Nanomechanics of carbon honeycomb cellular structures. *Carbon* **2017**, *113*, 26−32.

(14) Dikin, D. A.; Stankovich, S.; Zimney, E. J.; Piner, R. D.; Dommett, G. H. B.; Evmenenko, G.; Nguyen, S. T.; Ruoff, R. S. Preparation and characterization of graphene oxide paper. *Nature* **2007**, *448*, 457.

(15) Chen, H.; Müller, M. B.; Gilmore, K. J.; Wallace, G. G.; Li, D. Mechanically strong, electrically conductive, and biocompatible graphene paper. *Adv. Mater.* **2008**, *20*, 3557−3561.

(16) Park, S.; Lee, K.-S.; Bozoklu, G.; Cai, W.; Nguyen, S. T.; Ruoff, R. S. Graphene oxide papers modified by divalent ions—enhancing mechanical properties via chemical cross-linking. *ACS Nano* **2008**, *2*, 572−578.

(17) Liu, Y.; Xie, B.; Zhang, Z.; Zheng, Q.; Xu, Z. Mechanical properties of graphene papers. *J. Mech. Phys. Solids* **2012**, *60*, 591−605.

(18) Park, S.; Suk, J. W.; An, J.; Oh, J.; Lee, S.; Lee, W.; Potts, J. R.; Byun, J.-H.; Ruoff, R. S. The effect of concentration of graphene nanoplatelets on mechanical and electrical properties of reduced graphene oxide papers. *Carbon* **2012**, *50*, 4573−4578.

(19) Lee, W.; Lee, J. U.; Jung, B. M.; Byun, J.-H.; Yi, J.-W.; Lee, S.-B.; Kim, B.-S. Simultaneous enhancement of mechanical, electrical and thermal properties of graphene oxide paper by embedding dopamine. *Carbon* **2013**, *65*, 296−304.

(20) Shen, X.; Lin, X.; Yousefi, N.; Jia, J.; Kim, J.-K. Wrinkling in graphene sheets and graphene oxide papers. *Carbon* **2014**, *66*, 84−92.

(21) Xiao, Y.; Xu, Z.; Liu, Y.; Peng, L.; Xi, J.; Fang, B.; Guo, F.; Li, P.; Gao, C. Sheet collapsing approach for rubber-like graphene papers. *ACS Nano* **2017**, *11*, 8092−8102.

(22) Wang, S.; Gao, Y.; Wei, A.; Xiao, P.; Liang, Y.; Lu, W.; Chen, C.; Zhang, C.; Yang, G.; Yao, H.; Chen, T. Asymmetric elastoplasticity of stacked graphene assembly actualizes programmable untethered soft robotics. *Nat. Commun.* **2020**, *11*, 4359.

(23) Fang, M.; Wang, K.; Lu, H.; Yang, Y.; Nutt, S. Covalent polymer functionalization of graphene nanosheets and mechanical properties of composites. *J. Mater. Chem.* **2009**, *19*, 7098−7105.

(24) Kulkarni, D. D.; Choi, I.; Singamaneni, S. S.; Tsukruk, V. V. Graphene oxide-polyelectrolyte nanomembranes. *ACS Nano* **2010**, *4*, 4667−4676.

(25) Araby, S.; Zaman, I.; Meng, Q.; Kawashima, N.; Michelmore, A.; Kuan, H. C.; Majewski, P.; Ma, J.; Zhang, L. Melt compounding

with graphene to develop functional, high-performance elastomers. *Nanotechnology* **2013**, *24*, 165601.

(26) Gao, H.; Ji, B.; Jager, I. L.; Arzt, E.; Fratzl, P. Materials become insensitive to flaws at nanoscale: Lessons from nature. *Proc. Natl. Acad. Sci. U. S. A.* **2003**, *100*, 5597−5600.

(27) Ji, B.; Gao, H. Mechanical properties of nanostructure of biological materials. *J. Mech. Phys. Solids* **2004**, *52*, 1963−1990.

(28) Zhu, H.; Zhu, S.; Jia, Z.; Parvinian, S.; Li, Y.; Vaaland, O.; Hu, L.; Li, T. Anomalous scaling law of strength and toughness of cellulose nanopaper. *Proc. Natl. Acad. Sci. U. S. A.* **2015**, *112*, 8971−8976.

(29) Khan, U.; May, P.; O'Neill, A.; Coleman, J. N. Development of stiff, strong, yet tough composites by the addition of solvent exfoliated graphene to polyurethane. *Carbon* **2010**, *48*, 4035−4041.

(30) Xu, Z. Graphene composites. In *Graphene*, Zhu, H.; Xu, Z.; Xie, D.; Fang, Y., Eds.; Academic Press: Cambridge, 2018; pp 201−214.

(31) Liang, J.; Huang, Y.; Zhang, L.; Wang, Y.; Ma, Y.; Guo, T.; Chen, Y. Molecular-level dispersion of graphene into poly(vinyl alcohol) and effective reinforcement of their nanocomposites. *Adv. Funct. Mater.* **2009**, *19*, 2297−2302.

(32) Jiang, L.; Shen, X.; Wu, J.; Shen, K. Preparation and characterization of graphene/poly(vinyl alcohol) nanocomposites. *J. Appl. Polym. Sci.* **2010**, *118*, 275−279.

(33) Dai, Z.; Wang, Y.; Liu, L.; Liu, X.; Tan, P.; Xu, Z.; Kuang, J.; Liu, Q.; Lou, J.; Zhang, Z. Hierarchical graphene-based films with dynamic self-stiffening for biomimetic artificial muscle. *Adv. Funct. Mater.* **2016**, *26*, 7003−7010.

(34) Gao, E.; Cao, Y.; Liu, Y.; Xu, Z. Optimizing interfacial cross-linking in graphene-derived materials, which balances intralayer and interlayer load transfer. *ACS Appl. Mater. Interfaces* **2017**, *9*, 24830−24839.

(35) Hou, D.; Lu, Z.; Li, X.; Ma, H.; Li, Z. Reactive molecular dynamics and experimental study of graphene-cement composites: Structure, dynamics and reinforcement mechanisms. *Carbon* **2017**, *115*, 188−208.

(36) Cao, C.; Daly, M.; Chen, B.; Howe, J. Y.; Singh, C. V.; Filleter, T.; Sun, Y. Strengthening in graphene oxide nanosheets: bridging the gap between interplanar and intraplanar fracture. *Nano Lett.* **2015**, *15*, 6528−6534.

(37) Ramanathan, T.; Abdala, A. A.; Stankovich, S.; Dikin, D. A.; Herrera-Alonso, M.; Piner, R. D.; Adamson, D. H.; Schniepp, H. C.; Chen, X.; Ruoff, R. S.; Nguyen, S. T.; Aksay, I. A.; Prud'Homme, R. K.; Brinson, L. C. Functionalized graphene sheets for polymer nanocomposites. *Nat. Nanotechnol.* **2008**, *3*, 327−331.

(38) Rasool, H. I.; Ophus, C.; Klug, W. S.; Zettl, A.; Gimzewski, J. K. Measurement of the intrinsic strength of crystalline and polycrystalline graphene. *Nat. Commun.* **2013**, *4*, 7.

(39) Zhang, P.; Ma, L.; Fan, F.; Zeng, Z.; Peng, C.; Loya, P. E.; Liu, Z.; Gong, Y.; Zhang, J.; Zhang, X.; Ajayan, P. M.; Zhu, T.; Lou, J. Fracture toughness of graphene. *Nat. Commun.* **2014**, *5*, 3782.

(40) Zhang, T.; Li, X.; Gao, H. Designing graphene structures with controlled distributions of topological defects: A case study of toughness enhancement in graphene ruga. *Extreme Mech. Lett.* **2014**, *1*, 3−8.

(41) Zhang, T.; Li, X.; Gao, H. Defects controlled wrinkling and topological design in graphene. *J. Mech. Phys. Solids* **2014**, *67*, 2−13.

(42) Jung, G.; Qin, Z.; Buehler, M. J. Molecular mechanics of polycrystalline graphene with enhanced fracture toughness. *Extreme Mech. Lett.* **2015**, *2*, 52−59.

(43) Song, Z.; Artyukhov, V. I.; Wu, J.; Yakobson, B. I.; Xu, Z. Defect-detriment to graphene strength is concealed by local probe: the topological and geometrical effects. *ACS Nano* **2015**, *9*, 401−408.

(44) Qin, H.; Sun, Y.; Liu, J. Z.; Liu, Y. Mechanical properties of wrinkled graphene generated by topological defects. *Carbon* **2016**, *108*, 204−214.

(45) Shekhawat, A.; Ritchie, R. O. Toughness and strength of nanocrystalline graphene. *Nat. Commun.* **2016**, *7*, 10546.

(46) Toh, C.-T.; Zhang, H.; Lin, J.; Mayorov, A. S.; Wang, Y.; Orofeo, C. M.; Ferry, D. B.; Andersen, H.; Kakenov, N.; Guo, Z.; Abidi, I. H.; Sims, H.; Suenaga, K.; Pantelides, S. T.; Özyilmaz, B. Synthesis and properties of free-standing monolayer amorphous carbon. *Nature* **2020**, *577*, 199−203.

(47) Liu, F.; Ming, P.; Li, J. Ab initiocalculation of ideal strength and phonon instability of graphene under tension. *Phys. Rev. B: Condens. Matter Mater. Phys.* **2007**, *76*, 064120.

(48) Grantab, R.; Shenoy, V. B.; Ruoff, R. S. Anomalous strength characteristics of tilt grain boundaries in graphene. *Science* **2010**, *330*, 946−948.

(49) Yazyev, O. V.; Louie, S. G. Topological defects in graphene: Dislocations and grain boundaries. *Phys. Rev. B: Condens. Matter Mater. Phys.* **2010**, *81*, 195420.

(50) Cockayne, E.; Rutter, G. M.; Guisinger, N. P.; Crain, J. N.; First, P. N.; Stroscio, J. A. Grain boundary loops in graphene. *Phys. Rev. B: Condens. Matter Mater. Phys.* **2011**, *83*, 195425.

(51) Terrones, H.; Lv, R.; Terrones, M.; Dresselhaus, M. S. The role of defects and doping in 2D graphene sheets and 1D nanoribbons. *Rep. Prog. Phys.* **2012**, *75*, 062501.

(52) Wang, M. C.; Yan, C.; Ma, L.; Hu, N.; Chen, M. W. Effect of defects on fracture strength of graphene sheets. *Comput. Mater. Sci.* **2012**, *54*, 236−239.

(53) Wei, Y.; Wu, J.; Yin, H.; Shi, X.; Yang, R.; Dresselhaus, M. The nature of strength enhancement and weakening by pentagon-heptagon defects in graphene. *Nat. Mater.* **2012**, *11*, 759−763.

(54) He, L.; Guo, S.; Lei, J.; Sha, Z.; Liu, Z. The effect of Stone-Thrower-Wales defects on mechanical properties of graphene sheets - A molecular dynamics study. *Carbon* **2014**, *75*, 124−132.

(55) Zandiatashbar, A.; Lee, G. H.; An, S. J.; Lee, S.; Mathew, N.; Terrones, M.; Hayashi, T.; Picu, C. R.; Hone, J.; Koratkar, N. Effect of defects on the intrinsic strength and stiffness of graphene. *Nat. Commun.* **2014**, *5*, 3186.

(56) Wang, G.; Dai, Z.; Wang, Y.; Tan, P.; Liu, L.; Xu, Z.; Wei, Y.; Huang, R.; Zhang, Z. Measuring interlayer shear stress in bilayer graphene. *Phys. Rev. Lett.* **2017**, *119*, 036101.

(57) Dappe, Y. J.; Basanta, M. A.; Flores, F.; Ortega, J. Weak chemical interaction and van der Waals forces between graphene layers: A combined density functional and intermolecular perturbation theory approach. *Phys. Rev. B: Condens. Matter Mater. Phys.* **2006**, *74*, 205434.

(58) Tan, P. H.; Han, W. P.; Zhao, W. J.; Wu, Z. H.; Chang, K.; Wang, H.; Wang, Y. F.; Bonini, N.; Marzari, N.; Pugno, N.; Savini, G.; Lombardo, A.; Ferrari, A. C. The shear mode of multilayer graphene. *Nat. Mater.* **2012**, *11*, 294−300.

(59) Wang, Z. J.; Dong, J.; Cui, Y.; Eres, G.; Timpe, O.; Fu, Q.; Ding, F.; Schloegl, R.; Willinger, M. G. Stacking sequence and interlayer coupling in few-layer graphene revealed by in situ imaging. *Nat. Commun.* **2016**, *7*, 13256.

(60) Geim, A. K.; Grigorieva, I. V. Van der Waals heterostructures. *Nature* **2013**, *499*, 419−425.

(61) Laves, F.; Baskin, Y. On the formation of the rhombohedral graphite modification. *Zeitschrift Für Kristallographie* **1956**, *107*, 337−356.

(62) Cui, T.; Mukherjee, S.; Sudeep, P. M.; Colas, G.; Najafi, F.; Tam, J.; Ajayan, P. M.; Singh, C. V.; Sun, Y.; Filleter, T. Fatigue of graphene. *Nat. Mater.* **2020**, *19*, 405−411.

(63) Plimpton, S. Fast parallel algorithms for short-range molecular dynamics. *J. Comput. Phys.* **1995**, *117*, 1−19.

(64) Stuart, S. J.; Tutein, A. B.; Harrison, J. A. A reactive potential for hydrocarbons with intermolecular interactions. *J. Chem. Phys.* **2000**, *112*, 6472−6486.